International Forum on Aeroelasticity and Structural Dynamics
IFASD 2019
9-13 June 2019, Savannah, Georgia, USA

AN INTEGRATED ANALYSIS MODEL FOR ASSESSMENT OF CRITICAL LOAD CONDITIONS FOR THE VERTICAL TAIL PLANE

Thiemo M. Kier[1], Reiko Müller[1], Gertjan Looye[1]

[1]German Aerospace Center, DLR
Institute of System Dynamics and Control
82234 Weßling, GERMANY
Thiemo.Kier@dlr.de
Reiko.Mueller@dlr.de
Gertjan.Looye@dlr.de

Abstract: This paper presents a modelling scheme suitable for loads analysis of manoeuvres and gusts of a flexible controlled aircraft. In contrast to most ongoing research, the component to be investigated is not the wing but the vertical tail plane (VTP).

Critical load conditions for vertical tail plane include yawing maneoeuvre conditions as well as discrete lateral gusts. The resulting design loads are heavily influenced by the flight control system and the associated parameters for yaw damping functions or travel limiter. This poses an interesting problem regarding trade-offs between handling qualities and the structural loads acting on the VTP. This paper investigates the influence of lateral flight control laws on the loads of the different gust and manoeuvre load conditions for certification as specified by the authorities.

Sparked by previous incidents, a new load condition was recently introduced: the rudder reversal condition. This new condition features three full reversals of the rudder pedal input instead of just one step input and a mere return to neutral. The loads resulting from the new load condition are considered to be ultimate and not limit loads. The new load condition is assessed and compared to loads envelopes according to the old certification specifications. The introduction of the new rudder control reversal load condition was mainly motivated by wake vortex encounters during which the pilots made excessive or inappropriate use of the rudder. The conjecture is that the loads are primarily caused by pilot action and not the external windfield. Since the present modelling scheme is also capable of simulating position and attitude dependent windfields such as wake vortex encounters, the resulting loads are compared to the new rudder control reversal condition as well.

1 INTRODUCTION

The sizing loads for the aircraft structural components are determined by the so called loads analysis. Flight loads analysis, i.e. determining the dynamic loads that occur during flight is a field that plays an important role in the aircraft design process. For this many different load conditions at various points in the flight envelope and different payload/fuel combinations need to be simulated, which may amount to well over 1e5 load cases to be considered. Hence, there is the need for loop capable models which are fast, yet accurate to simulate all the different combinations of mass cases, flight points and load conditions that might become critical. The research community is typically focused on wing loads. Nevertheless, the vertical tail plane (VTP) is a very interesting component for loads analysis. There are many load conditions

specified in [1] that are important for the VTP, such as the yawing manoeuvre (CS 25.351), the one engine out condition (CS 25.367), as well as discrete lateral gusts and continuous turbulence (CS 25.341). The critical loads of the VTP are heavily dependent on the flight control laws, such as the yaw damper function and limitation of the rudder travel. Furthermore, there is a tradeoff between manoeuvre and gust loads depending on the employed control laws. The VTP is also the component most susceptible to overload conditions. Past flight incidents [2] initiated a new rule making process by the responsible authorities EASA [3] and FAA [4], where aircraft encountered wake vortex turbulence. The induced aircraft motion enticed the pilots to excessive use of the rudder, which in turn resulted in loads exceeding the design limit loads of the VTP [2]. The new paragraph CS 25.353 specifies a full-pedal command followed by three rudder reversals at the maximum sideslip angle before returning to neutral. This new paragraph is effective with the EASA CS-25 Amendment 22 [1], released on the 5th November 2018. At the time of this writing (20th May 2019) the rule was in the final rule stage at the FAA with a new release of a CFR 14 Part 25 amendment still pending. Currently, the yawing manoeuvre paragraph CS 25.351 only specifies one full pedal command with a return to neutral after a steady sideslip angle has been established. Since such occurrences are rare, the resulting loads may be regarded as ultimate loads, i.e. only a safety factor of 1.0 needs to be applied opposed to 1.5 for the limit load cases. This paper will present a summary of an integrated modelling scheme for gust and manoeuver loads of a flexible controlled aircraft [5, 6]. The components of the integrated modelling scheme will be recapped including rigid body and structural dynamics equations of motion. The aerodynamics model relies on linearized potential theory including unsteady aerodynamics by using the Doublet Lattice Method [7]. An overview of the flight control system will be provided with a particular focus on the lateral flight control laws.

A subset of load conditions relevant for VTP structural sizing will be presented: the discrete lateral gusts (CS 25.341(a)), the yawing manoeuvre (CS 25.351) and the newly introduced rudder control reversal condition (CS 25.351). The criticality of these load conditions for the VTP sizing depends on the aircraft type and also strongly on the flight control laws for lateral motion. Simulation results for different settings of the yaw damping gains will be presented, and the impact of the new rudder control reversal condition will be assessed.

The root cause for initiating the rudder reversal load condition where wake vortex encounters resulting in inadvertent rudder commands. The present integrated loads analysis model is also capable of simulating such wake encounters [6, 8]. While not in the regulations, dynamic loads resulting from such events can also be severe [9, 10]. The loads from wake encounter simulations will also be included in the loads envelopes of the VTP for comparison.

2 INTEGRATION OF LOADS ANALYSIS MODEL

The following section describes the general principles regarding the integration aspects of the loads analysis model, i.e., the structural model, the equations of motion, the external forces due to propulsion and the aerodynamics, and the flight control system. These equations are integrated in the loads environment VarLoads [11] and are expressed in closed form by the use of AIC matrices, i.e., no iteration between the structural and the aerodynamic model is necessary.

2.1 Structural Dynamics, Equations of Motion and Load Recovery

The starting point when setting up the equations of motion for a loads analysis model of a flexible aircraft is an Finite Element Model (FEM). This FEM usually consists of 100.000s of

degrees of freedom (DoFs). Static condensation can be used to reduce the problem size by several orders of magnitude. The method employed is known as the Guyan reduction [12], where condensation points ($g-set$) are placed along a loads reference axes. The mass distributions are prepared for the corresponding payload/fuel cases and connected to the $g-set$ points. Subsequently a modal analysis is carried out and only part of the modal basis is retained to further reduce the model size and computational cost.

The eigenvalues and eigenvectors define the generalized coordinates of the $h-set$. The zero eigenvalues represent the rigid body motion. The $h-set$ can be partitioned into six rigid body DoFs ($b-set$) and a flexible part ($f-set$). The rigid body mode shapes $\mathbf{\Phi}_{gb}$ and the retained modes of the eigenvector matrix $\mathbf{\Phi}_{gf}$ are used to generalized the equations of motion, which are given in the frequency domain by

$$\left\{-\omega^2 \begin{bmatrix} \mathbf{M}_{bb} & \mathbf{0} \\ \mathbf{0} & \mathbf{M}_{ff} \end{bmatrix} + \mathrm{j}\,\omega \begin{bmatrix} \mathbf{0} & \mathbf{0} \\ \mathbf{0} & \mathbf{B}_{ff} \end{bmatrix} + \begin{bmatrix} \mathbf{0} & \mathbf{0} \\ \mathbf{0} & \mathbf{K}_{ff} \end{bmatrix}\right\} \begin{bmatrix} \mathbf{u}_b \\ \mathbf{u}_f \end{bmatrix} = \begin{bmatrix} \mathbf{\Phi}_{gb}^{\mathrm{T}} \\ \mathbf{\Phi}_{gf}^{\mathrm{T}} \end{bmatrix} \mathbf{P}_g^{ext}(\omega). \tag{1}$$

Note that the rigid body $b-set$ DoFs in eq. (1) are defined in a earth fixed coordinate frame.

A suitable set of equations of motion to account for large rigid body motions and linear flexibility is derived in the references [13, 14]. The nonlinear equations of motion describe the movement relative to a "mean axes" body reference frame. Equations of motion for an unrestrained flexible aircraft accounting for large rigid body motions are given by

$$\begin{aligned} \begin{bmatrix} \mathbf{m}_b \left(\dot{\mathbf{V}}_b + \mathbf{\Omega}_b \times \mathbf{V}_b - \mathbf{T}_{bE}\, \mathbf{g}_E\right) \\ \mathbf{J}_b \dot{\mathbf{\Omega}}_b + \mathbf{\Omega}_b \times (\mathbf{J}_b \mathbf{\Omega}_b) \end{bmatrix} &= \mathbf{\Phi}_{gb}^{\mathrm{T}} \mathbf{P}_g^{\mathrm{ext}}(t) \\ \mathbf{M}_{ff}\ddot{\mathbf{u}}_f + \mathbf{B}_{ff}\dot{\mathbf{u}}_f + \mathbf{K}_{ff}\mathbf{u}_f &= \mathbf{\Phi}_{gf}^{\mathrm{T}} \mathbf{P}_g^{\mathrm{ext}}(t), \end{aligned} \tag{2}$$

where $\mathbf{\Phi}_{gb}$ is the rigid body modal matrix about the center of gravity and in directions as customary in flight mechanics, i.e., x-forward, z-down. $\mathbf{V}_b$ and $\mathbf{\Omega}_b$ are the velocity and angular velocity vectors, respectively in the body frame of reference. The matrix $\mathbf{T}_{bE}$ transforms the gravitational vector from an earth fixed (E) to the body fixed coordinate frame (b) as a function of Euler angles.

In order to recover the nodal loads $\mathbf{P}_g$ for a subsequent sizing of the structure, the force summation method (FSM) [15] is employed. Thus, subtraction of the inertial loads $\mathbf{P}_g^{\mathrm{iner}}$ from the external loads, yields

$$\mathbf{P}_g = \mathbf{P}_g^{\mathrm{ext}} - \underbrace{\mathbf{M}_{gg} \left\{\mathbf{\Phi}_{gb}\, \ddot{\mathbf{u}}_b \quad + \quad \mathbf{\Phi}_{gf}\, \ddot{\mathbf{u}}_f\right\}}_{\mathbf{P}_g^{\mathrm{iner}}} \tag{3}$$

In the case of the nonlinear equations of motion (2), the rigid body acceleration is given as

$$\ddot{\mathbf{u}}_b = \begin{bmatrix} \dot{\mathbf{V}}_b + \mathbf{\Omega} \times \mathbf{V}_b - \mathbf{T}_{bE}\, \mathbf{g}_E \\ \dot{\mathbf{\Omega}}_b + \mathbf{J}_b^{-1} \left(\mathbf{\Omega}_b \times (\mathbf{J}_b \mathbf{\Omega}_b)\right) \end{bmatrix}. \tag{4}$$

The FSM requires the external forces to be available in the structural DoF set ($g-set$). This allows to account for the static part directly on the physical grid, and therefore has a good convergence behavior. Then cut loads can be computed by integrating the nodal loads along the loads reference axes of each aircraft component. The envelope of the cut loads is used as sorting criteria to obtain the critical load cases used for the structural sizing.

2.2 Aerodynamic Model

The major contribution to the external forces apart from the propulsion forces stem from the aerodynamics. So called Aerodynamic Influence Coefficient (AIC) matrices based on linear potential flow theory have classically been used for aeroelastic applications. The AIC matrices represent a linear relationship between the normalwash at the control point to the panel pressure, i.e., a change of the flow, normal to the panel surface at control point results in a change in pressure distribution. This allows to easily account for flexible deformation, which are simply treated as change in the normalwash vector $\mathbf{w}_j$.

The pressure coefficients are computed by

$$\Delta \mathbf{c_p}_j = \mathbf{Q}_{jj}\ \mathbf{w}_j, \tag{5}$$

where $\mathbf{Q}_{jj}$ is the so called AIC matrix. Traditionally, the Vortex Lattice and the Doublet Lattice Methods are used to obtain these AIC matrices. The Doublet Lattice Method provides the complex valued AIC matrix as function of reduced frequency $k = \frac{c_{ref}/2}{U_\infty}\omega$, which describe the unsteady aerodynamic transfer functions. In frequency domain calculations the complex AICs can be used directly. For time domain simulations, a Rational Function Approximation (RFA) [5, 16] is required to transform the AICs to the Laplace domain. The rational functions can then be cast in the form of a system of linear ordinary differential equations amenable to time integration.

The load transformation to panel reference point is done by integrating the pressures, which is mostly a simple multiplication with the aerodynamic box area. In some classical aerodynamic panel methods, additional moments occur due to an offset between control point and pressure application point, cf. [17]. These are accounted for by introducing rotational degrees of freedom in the aerodynamic panel $(k-set)$ and the respective moment arms into the integration matrix $\mathbf{S}_{kj}$. Multiplication with the dynamic pressure yields the aerodynamic forces.

$$\mathbf{P}_k^{\text{aero}} = q_\infty\ \mathbf{S}_{kj}\ \mathbf{c_p}_j \tag{6}$$

Next, the boundary condition for the normalwash has to be considered:

$$\mathbf{w}_j(k) = \left(\mathbf{D^x}_{jk} + \frac{\mathrm{d}}{\mathrm{d}t}\left(\frac{c_{ref}/2}{U_\infty}\right)\ \cdot\ \mathbf{D^t}_{jk}\right)\ \mathbf{u}_k(t), \tag{7}$$

where the matrix $\mathbf{D^x}_{jk}$ accounts for a change in downwash due to tilting of the normal vector with respect to the free stream direction and the matrix $\mathbf{D^t}_{jk}$ for additional downwash due to movement of the boundary in direction of the panel normal. The factor $\frac{c_{ref}/2}{U_\infty}$ in equation (7) is needed due to the conversion from reduced to natural frequency. The vector $\mathbf{u}_k(t)$ represents the motion of the aerodynamic reference points.

When the nonlinear equations of motion are used, special attention to the boundary condition is required. The vectors $\mathbf{V}_b$ and $\mathbf{\Omega}_b$ are defined in a body fixed frame of reference. Hence, the steady deflection of rigid body modes does not induce aerodynamic loads. Therefore, the differentiation matrix $\mathbf{D^x}$ needs to be canceled for the rigid body modes.

Finally, the aerodynamic loads have to be mapped to the structural degrees of freedom. The matrix connecting the displacements of the structural grid $(g-set)$ to the aerodynamic grid $(k-set)$ is called spline matrix $\mathbf{T}_{kg}$.

$$\mathbf{u}_k = \mathbf{T}_{kg}\mathbf{u}_g \tag{8}$$

This mapping is achieved by, e.g., employing radial basis functions such as the commonly used Infinite Plate Spline (IPS) [18]. The aerodynamic loads can be mapped back onto the structure with the transpose of the spline matrix, based on the principal of virtual work.

$$\mathbf{P}_g^{\text{aero}} = \mathbf{T}_{kg}^{\text{T}} \mathbf{P}_k^{\text{aero}} \tag{9}$$

Similarly, the modal matrix $\mathbf{\Phi}_{gf}$ and its transpose connect the flexible part of the equations of motion (1) and (2) to the aerodynamic model.

2.3 Rational Function Approximation

The Doublet Lattice Method [7] provides aerodynamic matrices as tabulated values at discrete reduced frequencies. One possibility to make them amenable for time domain integration is the so called rational function approximation (RFA), where the frequency domain transfer functions are fit with suitable "rational" terms. These can then be Laplace transformed and cast in state space form. Many flavors of this method have been published in literature [16, 19, 20]. Most of these publications concentrate on approximation of the generalized aerodynamic matrices $\mathbf{Q}_{hh}$, i.e. the AIC matrices are already post-multiplied with the differentiation matrices (7) and the modal basis. This approach reduces the computational cost due to a smaller problem size.

In [5] an RFA fit of the AICs $\mathbf{Q}_{jj}(k)$ without prior multiplication with differentiation matrices was proposed, the so called "physical" RFA:

$$\mathbf{Q}_{jj}(\hat{s}) = \mathbf{Q^0}_{jj} + \mathbf{Q^1}_{jj}\hat{s} + \sum_{i=1}^{n_p} \mathbf{Q^{L}}_{i\,jj} \frac{\hat{s}\mathbf{I}}{\hat{s} + p_i}, \tag{10}$$

where $\hat{s} = s\left(\frac{c_{ref}/2}{U_\infty}\right)$ is the Laplace domain equivalent to the reduced frequency k. The reason for the presence of a second derivative in the classical RFA compared to the present formulation, is the additional time derivative in the downwash equation (7). The present, "physical" RFA (10) has several advantages over the approximation of the generalized aerodynamic forces, e.g., the fit is not tied to a particular mass case. But more importantly, the individual terms of the fit allow a physical interpretation: The term $\mathbf{Q^0}_{jj}$ represents the quasi-steady term, $\mathbf{Q^1}_{jj}$ is the added mass (in incompressible flow), and the terms $\mathbf{Q^{L}}_{i\,jj}$ with the predefined poles p_i, are responsible for the lagging behavior of the unsteady flow.

Since the input to the physical RFA is defined on the control point level, the gust velocity and the time lags associated with the penetration speed can be applied directly. The problematic approximation of the gust column can be omitted completely. Further, this fit also allows the consideration of a nonlinear position dependence of the wind field as demonstrated in [6], since the normalwash $\mathbf{w}_j$ can be computed online and fed into a realization of the ordinary differential equations (ODE) (11) of the unsteady aerodynamics in order to determine the so called lag states $\mathbf{x}_L$.

$$\dot{\mathbf{x}}_L = \frac{U_\infty}{c_{ref}/2}\mathbf{R}\,\mathbf{x}_L + \mathbf{E}\,\dot{\mathbf{w}}_j \tag{11}$$

The matrices $\mathbf{R}$ and $\mathbf{E}$ are stacked diagonal matrices, containing the poles p_i, respectively identity matrices. The splined aerodynamic forces including steady the unsteady parts are then

$$\mathbf{P}_g^{aero} = \underbrace{\left(\mathbf{Q^0}_{gj}\,\mathbf{w}_j\right)}_{\text{steady } \mathbf{P}_g^s(\mathbf{w}_j)} + \underbrace{\left(\mathbf{Q^1}_{gj}\left(\frac{c_{ref}/2}{U_\infty}\right)\,\dot{\mathbf{w}}_j + \mathbf{D}\,\mathbf{x}_L(\dot{\mathbf{w}}_j)\right)}_{\text{unsteady } \mathbf{P}_g^u(\dot{\mathbf{w}}_j)}, \tag{12}$$

where $\mathbf{D}$ contains the coefficients $\mathbf{Q}^{\mathbf{L}_i}{}_{gj}$ from the least squares procedure according to Roger [16]. With the "physical" RFA it is possible to discern between the steady and unsteady contribution of the aerodynamics, which is impossible when the fit is applied to the generalized aerodynamic forces.

2.4 Flight Control System

To realistically represent the behavior of an aircraft subjected to pilot inputs or atmospheric disturbances, the flight control system (FCS) also needs to be considered. The classical aeroelastic triangle [21] becomes an aeroservoelastic tetrahedron. The flight control system consists of sensors, which signals can then be processed by the flight control law implementations, and command control surface deflections via actuation systems. The flight control laws can alter the dynamics of the airframe and are present on all modern aircraft.

2.4.1 Flight Control Laws

The present flight control laws are designed according to the classical cascaded flight controller layout, where an inner loop captures fast states like aircraft orientation, and an outer loop or autopilot controlling slower states like flight path angle, course and speed. Since these variables change on different time scales, the two loops can be adjusted / tuned sequentially (instant attainment of faster states as seen by the outer loop and constant slower states as viewed from the inner loop). Furthermore, as longitudinal and lateral dynamics are only weakly coupled for a standard configuration fixed-wing aircraft, an additional separation into respective channels is possible in both loops.

For the considered scenarios, inner loop controllers for each the rolling, pitching and yawing motion with fixed structure have been implemented, while the outer loop / autopilot consists of the Total Energy Control System (TECS) and Total Heading Control System (THCS) formulations. The latter allow combined tracking of altitude and speed as well as course and sideslip angle respectively. In the case of the longitudinal autopilot/TECS, the energy conservation principle serves as basis for calculating pitch and throttle commands which balance potential and kinetic energy and regulate the total energy of the system.

The autopilot for the lateral motion / THCS similary adjusts roll angle and yaw rate commands in order to track commanded heading and sideslip angles, where the roll rate works to cancel the sum and the yaw rate to adjust the difference of the angle errors. Details on the concepts of TECS and THCS given in the original patent of Lambregts [22] and later adaptations [23, 24].

2.4.2 Yaw Damper and Rudder Travel Limiter

For the control of the yaw axis, the rudder control surface on the vertical tail plane is used. The rudder control surface has a variety of functions, where certain handling quality objectives must be met, e.g. to counteract crosswind or an engine failure during takeoff (V_{MCg}) on ground. To perform a crosswind approach and decrab the aircraft during the last phase of the landing to ensure alignment with the runway when flaring. When one engine is inoperative during fligh, the resulting yawing moment must be counteracted. This requirement is associated with the minimum control speeds V_{MCa} in the air and V_{MCl} during approach in landing configuration, where in clean and high lift configuration a sufficient yawing moment must be provided with no more than 5° bank angle (CS 25.149). During manoeuvres, rudder deflection is required for turn coordination to avoid lateral load factors due to sideslip. Furthermore, the lateral flight control law increases the damping of unwanted flight characteristics such as the dutch roll mode. The

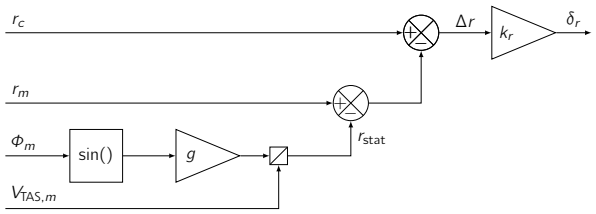

Figure 1: Yaw damper, which subtracts the stationary yaw rate for turning flight (r_{stat}) from measured yaw rate r_m. Similar to a high-pass filter, this yields the relevant frequencies of the Dutch-Roll motion.

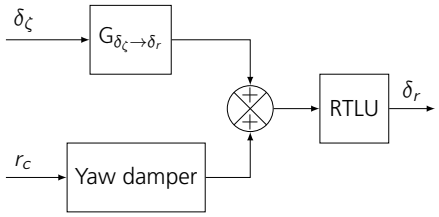

Figure 2: Rudder actuation through commands from pedals and yaw damper. The function $G_{\delta_\zeta \to \delta_r}$ translates pedal to rudder deflection commands

dutch roll is an eigenmode of the flight mechanics where rolling and yawing motion are coupled in an unfavorable way. Sometimes additional lateral flight control functions are implemented to enhance passenger comfort, e.g. mitigating the excitation of structural modes such as lateral fuselage bending through rudder usage.

These lateral flight control functions are implemented in the so called yaw damper, which augments the pilot yawing command (pedal input).

Figure 1 depicts the block diagram of an implementation of such a function. The measured yaw rate r_m is subtracted from a commanded yaw rate r_c issued either by the pilot or autopilot. The resulting error is proportionally applied to the rudder actuator as commanded yawing acceleration $k_r \cdot \Delta r$. However, since only disturbances due to the previously mentioned causes shall be damped, the stationary part of the yaw rate (which is for example present during turning flight) needs to be removed from the measured signal r_m. This can be done for example by employing a high-pass filter, or by directly subtracting the stationary turning rate $r_{\text{stat}} = \frac{g \cdot \sin \Phi_m}{V_{\text{TAS}}}$. The gain of the yaw damping function k_r determines the degree of attenuation.

Large rudder deflections incur high loads on the VTP structure, therefore the deflection is limited by a so called Rudder Travel Limitation Unit (RTLU). The deflection limit is scheduled as a function of the calibrated flight speed V_{CAS} to meet the pertaining handling quality requirements but at the same time avoid excessive loads on the VTP. It is applied to the sum of commands from pilot δ_ζ and yaw damper r_c, as shown in Figure 2.

3 CRITICAL DESIGN LOAD CONDITIONS FOR THE VERTICAL TAIL PLANE

Many paragraphs in the certification specifications are relevant for the structural sizing of the vertical tail, such as the one engine out condition (CS 25.367), lateral continuous turbulence (CS 25.341 (b)) as well as failure cases such as rudder runaways, oscillatory failures or force fighting of redundant rudder actuation systems. However, this paper focuses on the discrete tuned lateral gust (CS 25.341(a)) and the yawing manoeuvre condition (CS 25.351). These two conditions are exemplary for induced loads by external atmospheric disturbance, respectively by pilot control inputs.

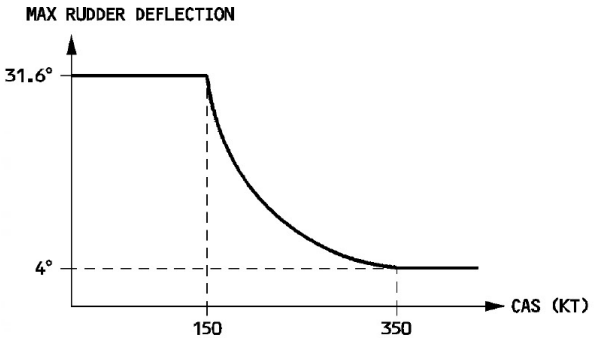

Figure 3: Maximum rudder deflection in dependence of V_{CAS}, used inside the RTLU

Furthermore, the newly introduced rudder control reversal condition (CS 25.353) is described and contrasted to the existing yawing manoeuvre paragraph CS 25.351.

3.1 Discrete Tuned Lateral Gust Condition

The paragraph for the analysis of lateral gusts evolved from using a Pratt type formula to the rational analysis of a discrete gust with varying gust wave lengths. Thereby, the lateral gust regulations followed a similar path of evolution to the vertical gust paragraphs. The vertical gust were originally described by the so called Pratt gust [25], taking into account a sudden change of angle of attack due to the gust velocity, resulting in an additional load factor n_z increment. The fact that the sharp edged gust induces more loads than a smooth gust profile was accounted for by an alleviation factor.

Later in JAR-25 change 13 from 5th October 1989 [26], a 1-cosine gust shape of a fixed gust length of 25 semi-chords was specified. Note that the mean geometric and not the mean aerodynamic chord is used as reference length. In JAR-25 change 14 from 27th May 1994 [27] the gust and turbulence paragraphs were harmonized [28], originally issued as so called orange paper amendments. The gust paragraph CS 25.341 was no longer solely responsible for symmetric vertical gust but also included the lateral gust conditions. The gust gradient lengths of 1-cosine shape now have to be varied between 30 and 350 ft. Furthermore section b) was introduced, a Continuous Turbulence Design Criteria where the response to the statistical von Karman power spectrum given in the frequency domain needs to be considered.

The lateral gust criterion in JAR-25 change 13 was originally formulated in paragraph JAR 15.351(b) Lateral Gusts. The Pratt type formula simply considered the side force L_t due to a gust, where K_{gt} is the gust alleviation factor with the lateral mass ratio μ_{gt}.

$$L_{\mathrm{t}} = \frac{K_{\mathrm{gt}}\, U_{\mathrm{de}}\, V\, S_{\mathrm{t}}}{498} \quad ; \quad K_{\mathrm{gt}} = \frac{0.88\,\mu_{\mathrm{gt}}}{5.3 + \mu_{\mathrm{gt}}} \quad ; \quad \mu_{\mathrm{gt}} = \frac{2\,W}{\rho\,\bar{c}_{\mathrm{t}}\,g\,a_{\mathrm{t}}\,S_{\mathrm{t}}} \left(\frac{K}{l_{\mathrm{t}}}\right)^2$$

U_{de} is the derived gust velocity (ft/s), ρ is the air density ($\mathrm{slugs/ft^3}$), W the aeroplane weight (lb), S_{t} is the area of vertical tail ($\mathrm{ft^2}$), $\bar{c}_{\mathrm{t}}$ is the mean geometric chord of vertical surface (ft), a_{t} is the lift curve slope of vertical tail (per radian), K the radius of gyration in yaw (ft), l_{t} is the distance from aeroplane c.g. to lift centre of vertical surface (ft), g is the acceleration due to gravity ($\mathrm{ft/s^2}$) and V is the aeroplane equivalent speed (knots).

Paragraph CS 25.341(a) nowadays features a discrete 1-cosine shaped gust profile. Gust gradient distances H in the range 30 ft to 350 ft must be considered to determine the critical response,

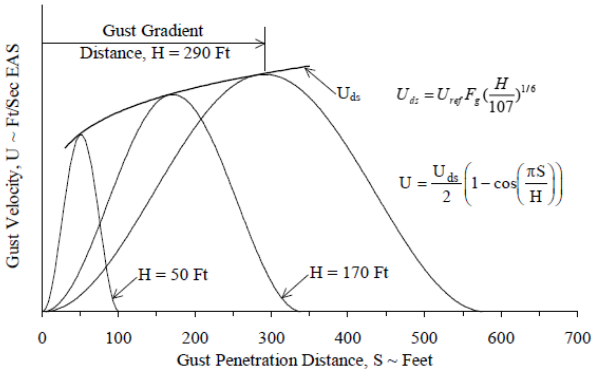

Figure 4: gust shape from AMC 25.341 of CS-25 [1]

cf. figure 4.

$$U = \frac{U_{\mathrm{ds}}}{2}\left(1 - \cos\left(\frac{\pi\, S}{H}\right)\right),$$

where the design gust velocity is given by

$$U_{\mathrm{ds}} = U_{\mathrm{ref}} F_{\mathrm{g}} \left(\frac{H}{107}\right)^{\frac{1}{6}}.$$

The reference gust velocity U_{ref} is linearly interpolated as function of altitude, starting from 56 ft/s at sea level, 44 ft/s at 15000 ft and 20.86 ft/s at 60000 ft. For the aeroplane design speed V_D the reference gust velocity is half of this value.

Hence, the design gust velocity varies with the gradient distance and a so called flight profile alleviation factor, which depends on the design weights of the aircraft type. The value for the flight profile alleviation factor is

$$F_g = \tfrac{1}{2}\left(1 - \frac{z_{\mathrm{mo}}}{76200} + \sqrt{\frac{m_{\mathrm{MLW}}}{m_{\mathrm{MTOW}}} \tan\frac{\pi}{4}\frac{m_{\mathrm{MZFW}}}{m_{\mathrm{MTOW}}}}\right),$$

where z_{mo} is the maximum operating altitude. All velocities are given in equivalent airspeed (EAS) and have to be converted to true airspeed (TAS) in the corresponding altitude.

For the gust load computations unsteady aerodynamics need to be taken into account. Gust loads analysis is usually carried out in the frequency domain, since the doublet lattice method readily provides the AIC matrices complex form as function of the reduced frequency parameter k. In this paper the analysis is done in the time domain, as it conveniently allows provision for nonlinearities in control systems.

3.2 Yawing Manoeuvre Condition

The yawing manoeuvre is a pilot induced load condition. Besides the unsymmetrical loads due to engine failure of CS 25.367, which is not considered in this paper, the yawing manoeuvre results in the large torsional loads on the vertical tail plane structure due to pedal input of the pilot.

The yawing manoeuvre needs to be considered between the minimum control speed V_{MC} and the design dive speed V_{D}. It can be characterized by four different phases:

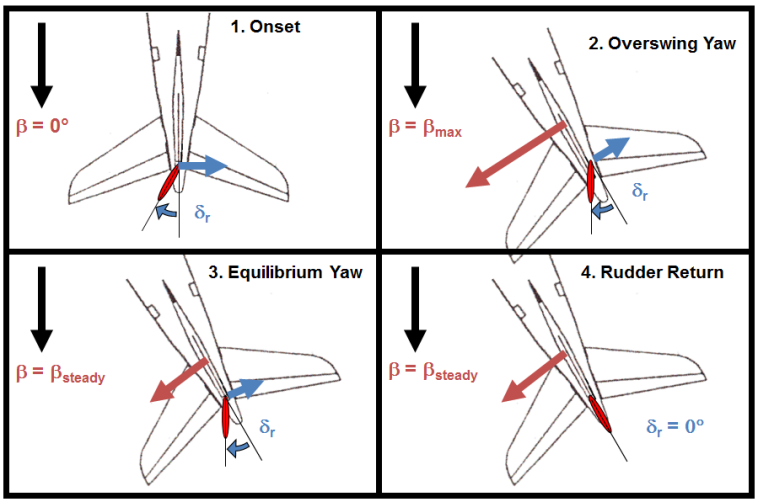

Figure 5: Yawing manoeuvre: four phases

1. **Onset**: Starting from level flight, the rudder is deflected by a sudden pilot pedal command.
2. **Overswing**: As a result of the rudder command the aircraft starts to yaw and a dynamic overswing resulting in a maximum sideslip angle occurs.
3. **Equilibrium Yaw**: Continuing the full rudder command, a state of constant sideslip is reached.
4. **Rudder Return**: Form the steady sideslip condition, the rudder command is returned to zero.

The occurring loads of the yawing manoeuvre heavily depend on the active lateral control law in particular the yaw damping function and the travel limit of the rudder control surface deflection.

3.3 Rudder Control Reversal Condition

A brand new paragraph is the CS 25.353 rudder control reversal condition. It is included in amendment 22 of the EASA CS 25, released on 5th November 2018. The FAA rule making process is the final stage, however an update of the 14 CFR Part 25 including the new paragraph has not been released yet (as of 20th May 2019).

The rudder reversal is a second yawing manoeuvre condition also involving rudder pedal inputs by the pilot. The chosen name seems to be somewhat unfortunate, since a reversal condition is usually associated with the aeroelastic phenomenon and not with an alternating pilot input, which might lead to a confusion. The new load condition consist of two full rudder doublets as opposed to only one rudder input as in CS 25.351. Furthermore, instead of reversing the controls at a steady sideslip angle, the rudder command has to be reversed at the maximum sideslip angle, which further increases the loads on the VTP. The onset of the manoeuvre of CS25.353 is addressed in subparagraph (a), the three control reversals in (b), (c) and (d), and finally the return of the rudder control to neutral in subparagraph (e), as depicted in figure 6.

In contrast to the yawing manoeuvre CS 25.351, only speeds between minimum control speed V_{MC} and design cruise speed V_{C} need to be considered.

The new load condition was introduced because incident investigations showed that pilots may make inadvertent or inappropriate rudder inputs during severe external disturbances, e.g. due to

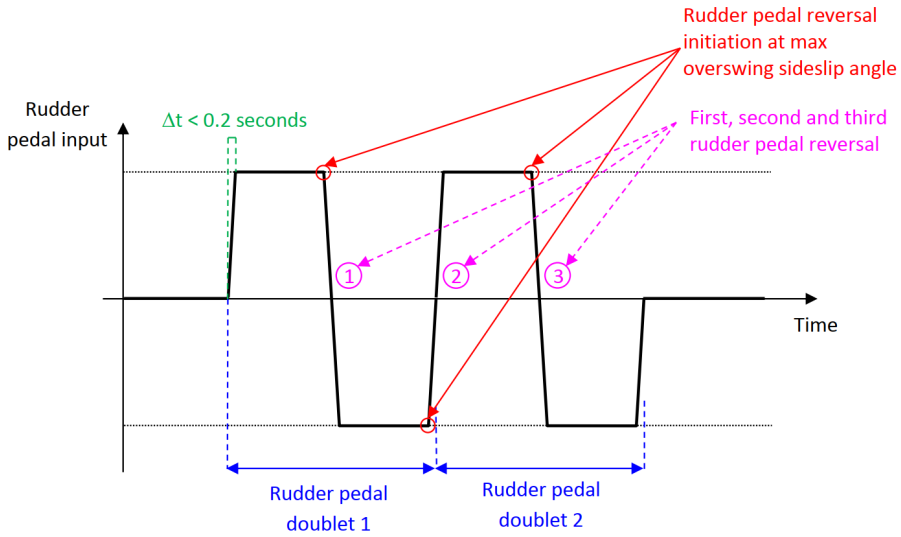

Figure 6: : CS 25.353 Rudder control reversal load condition as depicted in [1]

wake vortex encounters, in order to avoid upset flight conditions. Since the rate of occurrence for such incidences was deemed to be low, the loads resulting from such rudder reversals can be considered ultimate, i.e. the factor of safety of 1.5, as specified in CS 25.303, does not need to be applied.

4 SIMULATION RESULTS

The model used for the present study is one of a generic long range aircraft with two engines. Only one mass case is considered and also only the flight at the V_C/M_C intersection is covered. At this point in the flight envelope the gust velocity is not reduced and the dynamic pressure is large. Also the new rudder reversal manoeuvre condition only needs to be considered up to V_C. So the computed loads do not necessarily represent a design loads envelope but should be representative in terms of the resulting loads levels.

Nine different gust gradient lengths are considered for the discrete gust condition, where only a subset will be displayed individually for clarity. The yawing manoeuvre condition complements the gust loads for the design cases according to the status of CS-25 Amndt. 21 [29]. The resulting loads are then compared to those of the newly introduced the rudder control reversal condition.

As stated before the resulting loads are very sensitive to the chosen lateral control law. Therefore, different gains for the yaw damping function are assessed. One for a critically damped yawing motion ($k_r = 2.0$), i.e. no overswing in sideslip angle, one undamped control law without rudder action due to yaw rate ($k_r = 0.0$), and an intermediate damping gain with some overswing behavior ($k_r = 0.5$). Some qualitative remarks about the influence of the rudder travel limiter inhibiting the maximum deflection are made.

The comparison for the three different yaw damper gains is based on the correlation of bending and torsion moment loads at the VTP root. Furthermore, a hierarchy of the critical cases for the shear, bending and torsion moment along the VTP component axis is shown.

4.1 Lateral Discrete Gust

First, the lateral gust hits the front of the aircraft resulting in a yawing motion away from the gust. When the gust arrives at the vertical tail, the aircraft nose points into the direction of the

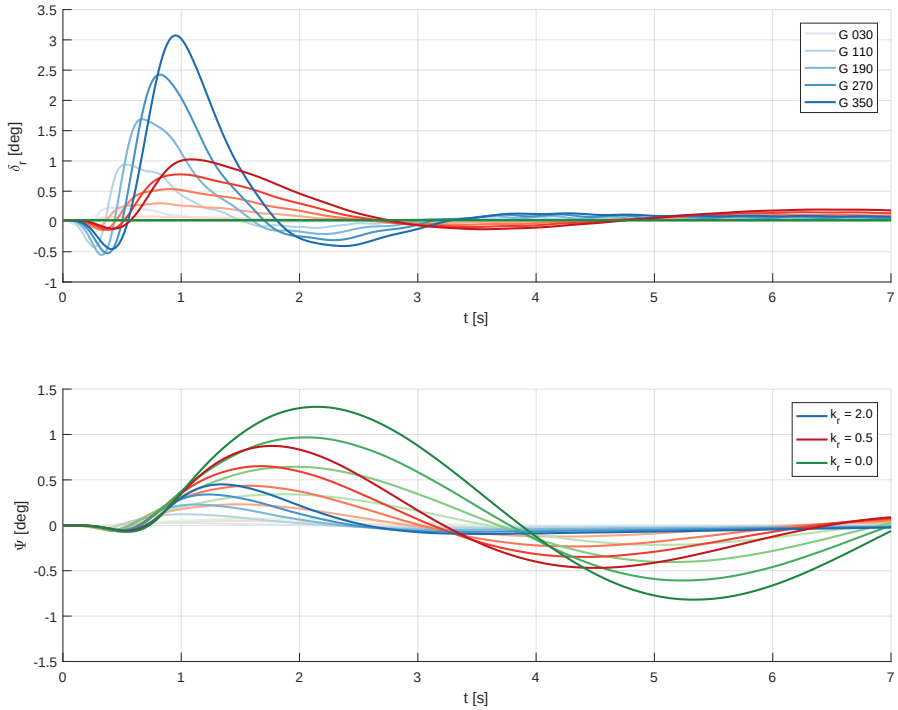

Figure 7: Rudder deflection and heading angle during lateral discrete gust

gust. The yaw damper deflects the rudder accordingly, as shown in figure 7. Longer gradient distances are accompanied by larger gust velocities. Therefore, larger yaw rates are induced which in turn result in more rudder deflection. Another contributing factor is of course that the reaction time for shorter gusts is constrained by sensor delays and actuator rates of the flight control system. The amount of rudder deflection depends on the yaw damper gains k_r. In the undamped case ($k_r = 0.0$) no rudder action is observed, leading to a significantly larger response of the heading angle. It should also be noted that the rudder deflections are well within the limits of the RTLU. Figure 8 depicts for the three different yaw damper gains the individual traces of the correlated bending and torsion moments for various gust gradient lengths at the VTP root. The envelopes are determined by a 2D convex hull of all traces including their mirrored counterpart, i.e. gust from the left and from the right hand side. The loads envelopes in figure 8 show that more rudder deflection helps to decrease the bending moment at the cost of an increase in torsion moment. The discrete gust is usually more critical for the bending moment, so the yaw damper helps in this case. The longer gradient distances usually result in higher bending moment loads. However, the longest gust gradient distance is not necessarily the most critical one, underlining the necessity for the gust tuning to determine the sizing load cases.

4.2 Yawing Manoeuvre

The yawing manoeuver consist of four individual phases spanning the correlated loads envelope. Fist the initial onset of the rudder deflection causes a negative bending moment with an associated positive torsion. Depending on magnitude of the yaw damping gain, the initial rudder deflection is taken back to reduce the overshoot of the sideslip angle. The maximum sideslip angle is the second characteristic point spanning the loads envelope, where the maximum torsion moment occurs. When the oscillations of the overshoot subside, a steady sideslip angle establishes. This constitutes phase three of the yawing manoeuvre. If the yaw damper critically damps the buildup of the sideslip, this phase coincides with the previous point in the

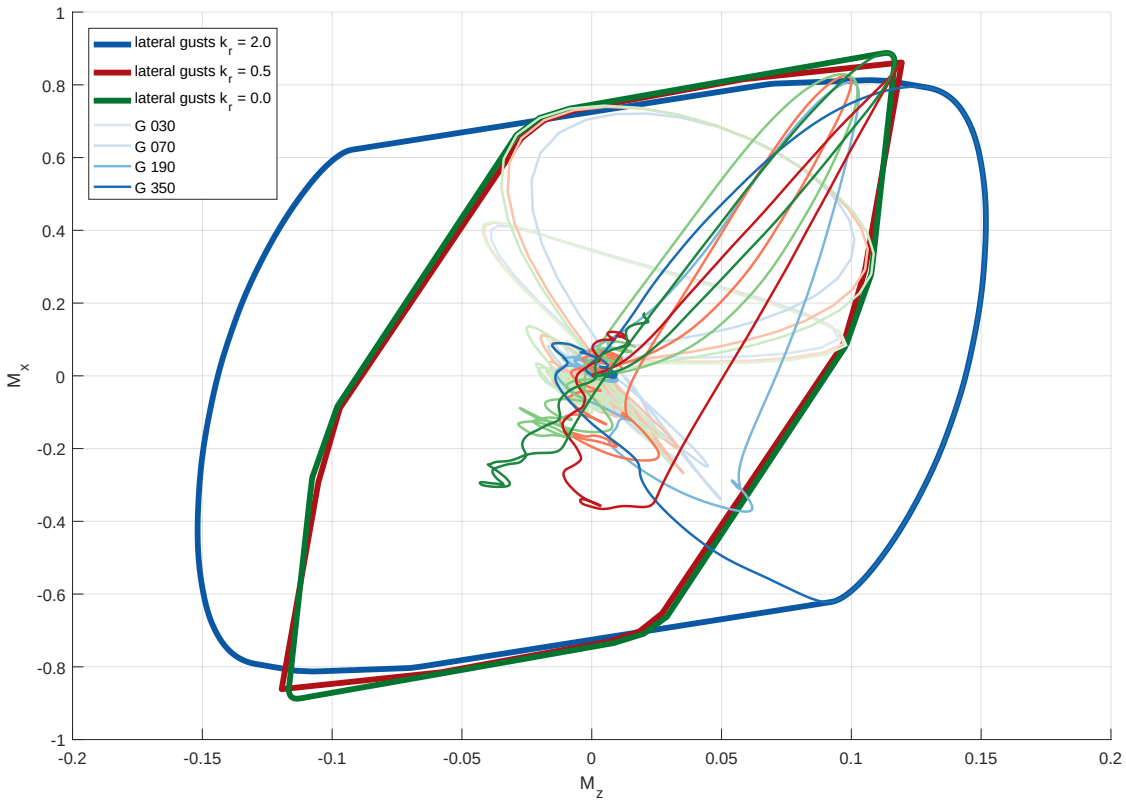

Figure 8: Correlated bending torsion moment loads for lateral discrete gust with different yaw damping gains

envelope. In phase four, the pedal input is returned to neutral. This is the phase where the maximum bending moment occurs, since the counteracting force due to rudder deflection is suddenly absent. This seems somewhat counterintuitive but can be regarded as an opposite rudder command superimposed with the already prevailing bending moment load due to the steady sideslip angle.

The graphs for rudder deflection δ_r, sideslip angle β, and the bending and torsion loads M_x and M_z versus time can be found in figure 10.

The loads resulting from the yawing manoeuvre are heavily influenced by the flight control system. High gains in the yaw damping function inhibit the β overswing. The largest sideslip angle β is responsible for the maximum torsion moment. Further, the RTLU sets limits to the allowable rudder deflection, which reduces the maximum achievable side slip angle and hence the bending and torsion loads. In phase four of the yawing manoeuvre, when the pilot command returns to neutral, the maximum bending moment is induced. This is also directly related to the maximum allowable rudder deflection, since the maximum bending moment occurs due to superposition of the achievable sideslip and the missing counter force of the rudder.

Reducing the allowable rudder deflections reliefs the loads on the vertical tail, however, this has to be balanced with the handling requirements where sufficient rudder deflection is necessary to counteract the yawing moment of a one engine inoperative condition, as well as for turn coordination. Figure 9 shows the traces of the correlated loads of the yawing manoeuvre for the different yaw damper gains. When combining the envelopes of manoeuvre and discrete gusts confirms the trends explained above – higher yaw damping gains reduce the overall loads. Also note that for the higher yaw damping $k_r = 2.0$ the discrete gust becomes critical for the

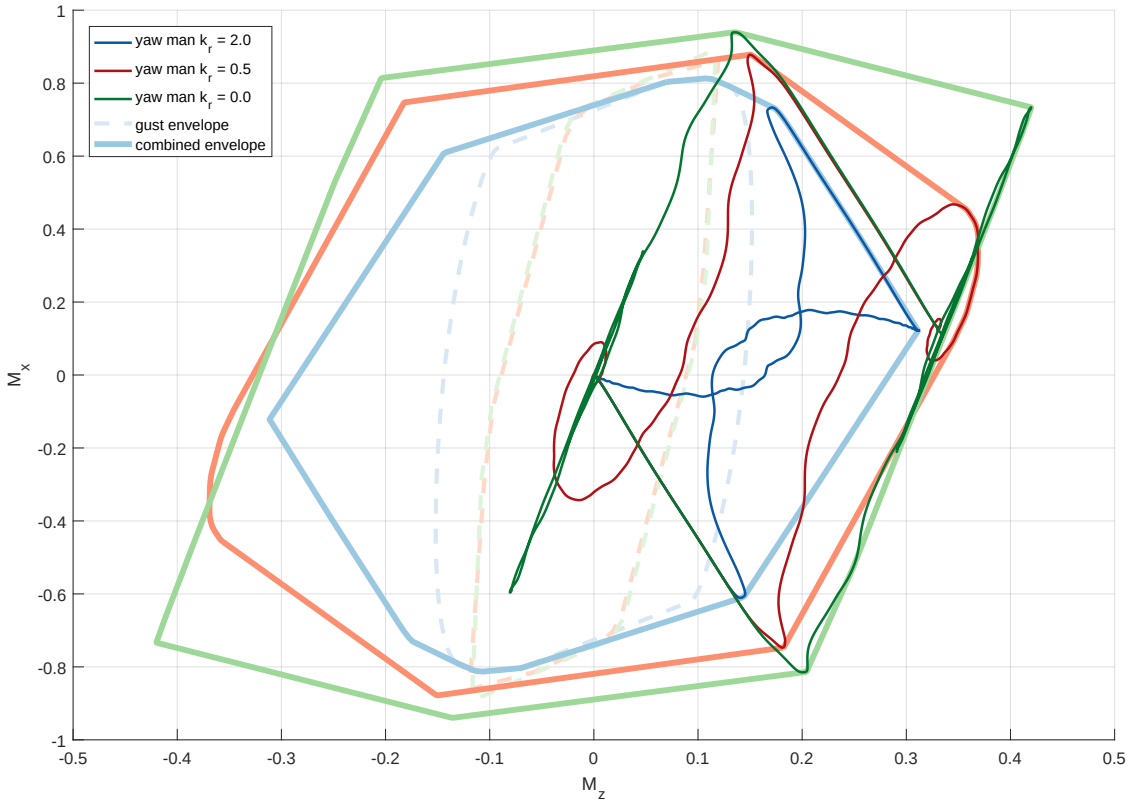

Figure 9: Correlated bending torsion moment loads for yawing manoeuvre with different yaw damping gains

bending moment. For the intermediate damping $k_r = 0.5$, the maximum bending moments of manoeurvre and gusts are approximately on par. For the undamped case $k_r = 0.0$ the bending is dominated by the manoeuvre.

4.3 Rudder Reversal

The newly introduced rudder reversal condition CS 25.353 consists of two full rudder doublets in contrast to the single pedal input of the conventional yawing manoeuvre condition of CS 25.351. Figure 10 depicts the rudder deflection, the sideslip angle and the resulting bending and torsion loads for the rudder control reversal as well as the conventional yawing manoeuvre.

The initial onset of the rudder reversal condition is equal to the conventional yawing manoeuvre. Also, the rudder return causes the highest loads, just like in the conventional yaw manoeuvre, but this time the pedal input is not only commanded to return to neutral but to the maximum opposite deflection, which results in extremely large bending moments.

Furthermore, the reversing pedal input is required to be initiated at the maximum sideslip angle, instead of the steady state value. When overcritical yaw damping gains ($k_r = 2.0$) are employed, the successive opposite deflections do not result in any higher loads compared to a single doublet and simply follow the same trajectory in the correlated loads plot a second time. However, in the case of low yaw damping, this leads to extremely high loads. For aircraft types with a high inertia around the z-axis, these loads are so large that even when considered as ultimate loads, they are most likely prohibitive for any kind of lateral control law design with undercritical yaw damping.

Figure 11 shows the bending torsion correlated loads envelopes without the new rudder reversal condition. The traces of the rudder reversal manoeuvres are scaled down by a factor of 1.5

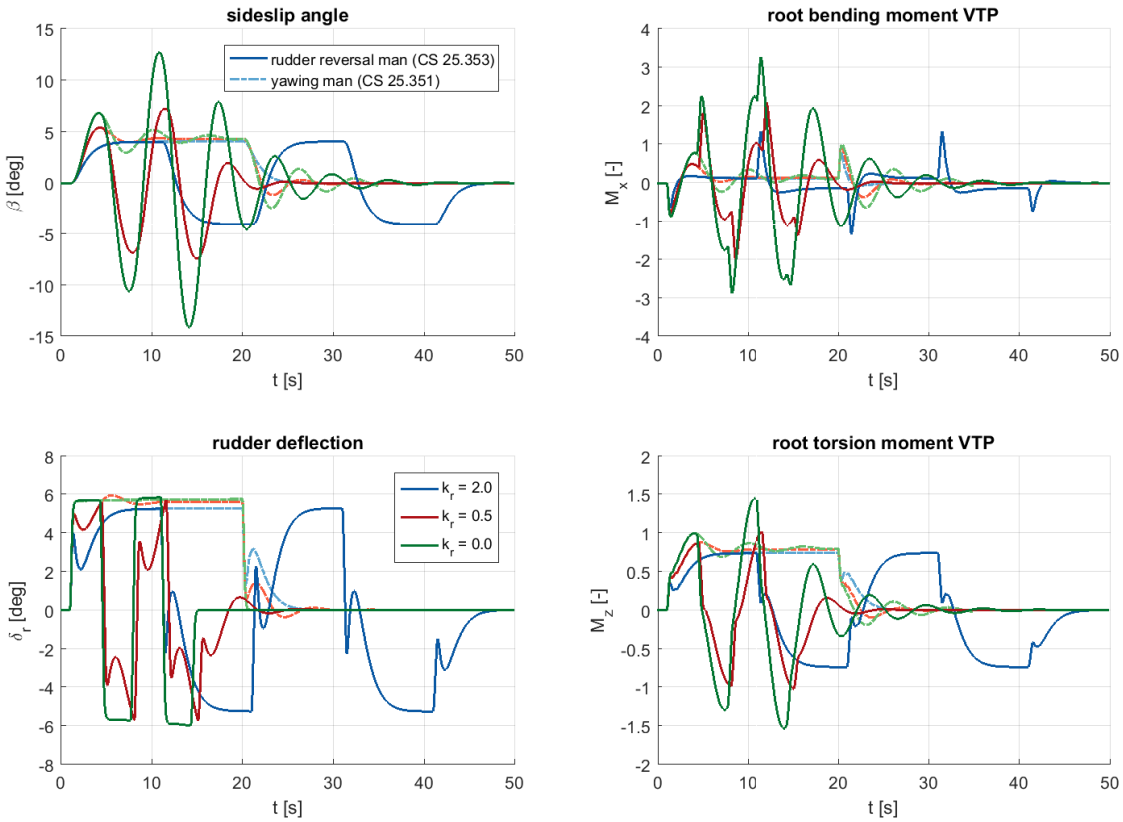

Figure 10: Rudder Reversal Responses: sideslip rudder deflection and bending and torsion moment loads with different yaw damping gains

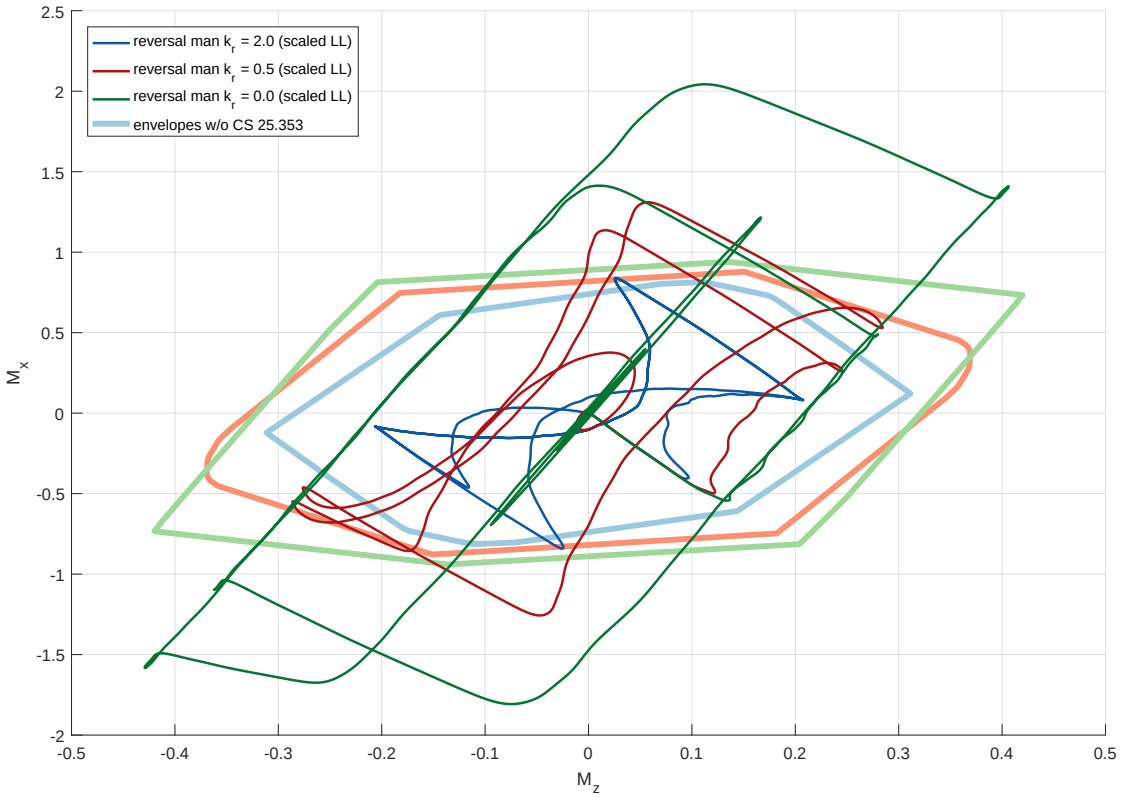

Figure 11: Correlated bending torsion moment loads for rudder control reversal manoeuvre with different yaw damping gains

to constitute limit loads to assess their impact on design loads envelopes. In the case of the critically damped case, the correlated loads envelope is not expanded by a large amount and most likely covered by either other load conditions, or not completely exhausted reserve factors of the structure. For the lower yaw damping gains the loads for heavy aircraft types induced by the new load condition are severe and most likely have impact on the lateral control law design. It should be noted that this assessment is based on generic aircraft data and not on a particular aircraft or real aircraft control system and by no means conclusive. It simply is meant to show the impact of the new paragraph on the resulting loads levels and on control law design strategies.

4.4 Loads hierarchy along the VTP component axis

So far only quantities of flight mechanics and loads at the VTP root were considered. It is important and also instructive to observe the integrated loads along the component axis. Therefore, one dimensional load envelopes are computed for the integrated shear, bending moment and torsion load quantities, the so called SMT plots. To assess the hierarchy of load cases the individual cases are divided by the maximum value in the envelope. This way trades between different load conditions can be easily assessed and trades between different design parameters lowering one condition but increasing another can be made. The resulting loads hierarchy for a yaw damping gain of $k_r = 2.0$ is shown in figure 12.

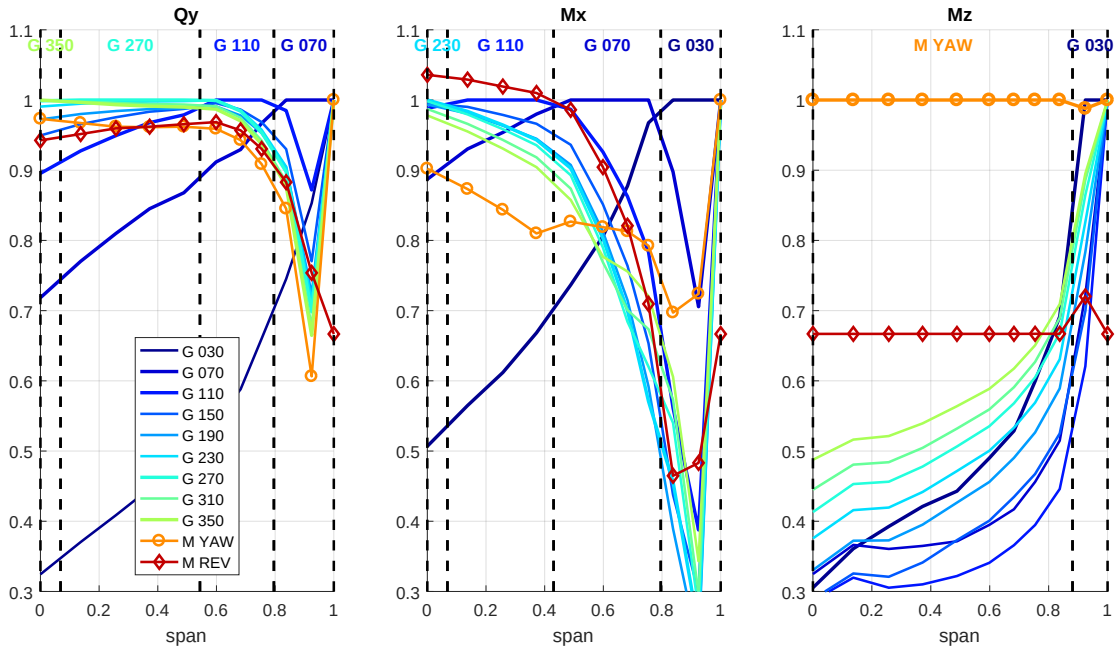

Figure 12: Correlated bending torsion moment loads for rudder control reversal manoeuvre with different yaw damping gains

As expected the torsion moment is dominated by the yawing manoeuvre condition. For the shear force and the bending moment the discrete gusts are more critical. The root is sized by the longer gradient distances, moving along to the tip shorter gust become more critical. Even for the torsion moment the shortest gust length becomes critical, however this is likely not relevant due to minimum skin thickness manufacturing constraints.

The loads due to the rudder reversal are scaled down by a factor of 1.5 to represent limit loads. Here, the bending moment is sized by the new load condition case approximately between root and mid span. The loads at the root are about 4 % higher compared to the envelope without

the new load condition. The shear force of the rudder reversal is approximately on par with the conventional yawing manoeuvre at about 95 % limit load.

5 WAKE VORTEX ENCOUNTER

The primary reason of the introduction of the new load condition was the observed reaction of pilots during wake vortex encounters. The induced aircraft motion during such encounters enticed the pilots to excessive use of the rudder, including several control reversals. The loads solely from this type of manoeuvre can result in exceedance of the design limit loads, hence the new load condition was established to cover such scenarios. The conjecture is that loads are dominated by the pilot input and not by the external wind field. Depending on the encounter angle the response can be more manoeuvre like (by the induced rolling motion of the vortex) for acute encounter angles or more gust like (rapidly changing vertical wind field) for obtuse encounter angles. The described modelling scheme has already been successfully applied to wake vortex encounters [6, 8, 9].

5.1 Wake Vortex Encounter Scenario

Two cases of wake vortex encounters are presented here, one open loop and one with auto pilot engaged. This is of course not representative of pilot responses but can give hints what the induced loads due an external disturbance such as wake vortex encounters can be.

It should further be noted that the applied control surface deflections in the case of the closed loop simulation were not limited. Neither was there a proper allocation for the roll control function. Usually for higher speeds and Mach numbers the ailerons are deflected less in favor of roll spoiler deflections due to buffeting and aeroelastic control reversal considerations.

A multitude of WVE scenarios are possible regarding crossing angles, vertical offsets, wake geometry and circulation strengths. The scenario selected here matches closely the circumstances of flight AC190 in the report [2]. There, an Airbus A319 at flight level 370 with a speed of 450 KTAS crossed a wake generated by a Boeing 747-400. The encounter angle was 3° and resulted in violent motion. During the event (duration of 18 s) with four oscillations, the heading varied by 21 degrees. The vertical accelerations reached peak values of +1.57g and -0.77g, the lateral acceleration went from +0.49g (right) to -0.46g left.

The weight of the vortex generating aircraft was assumed to be $m_G = 400000\ \mathrm{kg}$, the speed of $490\ \mathrm{KTAS}$ at flight level 370 corresponds to $V_G = 250\ \mathrm{m/s}$. The wing span of a Boeing 747-400 is $b_G = 64.4\ \mathrm{m}$ This results in a circulation strength of the generated wake vortex of approximately

$$\Gamma_w = \frac{m_G \cdot g}{\rho \cdot V_G \cdot b_G \frac{\pi}{4}} \approx 880\ \mathrm{m^2/s}.$$

For the encountering aircraft a generic short range aircraft model is selected, crossing the wake at an angle of 3°, i.e. a very acute angle triggering a manoeuvre type response

5.2 Design Loads and WVE Results

For this wake vortex simulation a generic short range aircraft was used, instead of the long range type. First the generic short range aircraft is subjected to the same load conditions described in the previous chapter. The yaw damper gain for this aircraft was set to $k_r = 0.5$. Short range aircraft has a considerably lower I_{zz} mass moment of inertia and therefore experience substantial yaw rates during gust encounters. If a high yaw damper is chosen, the rudder deflection

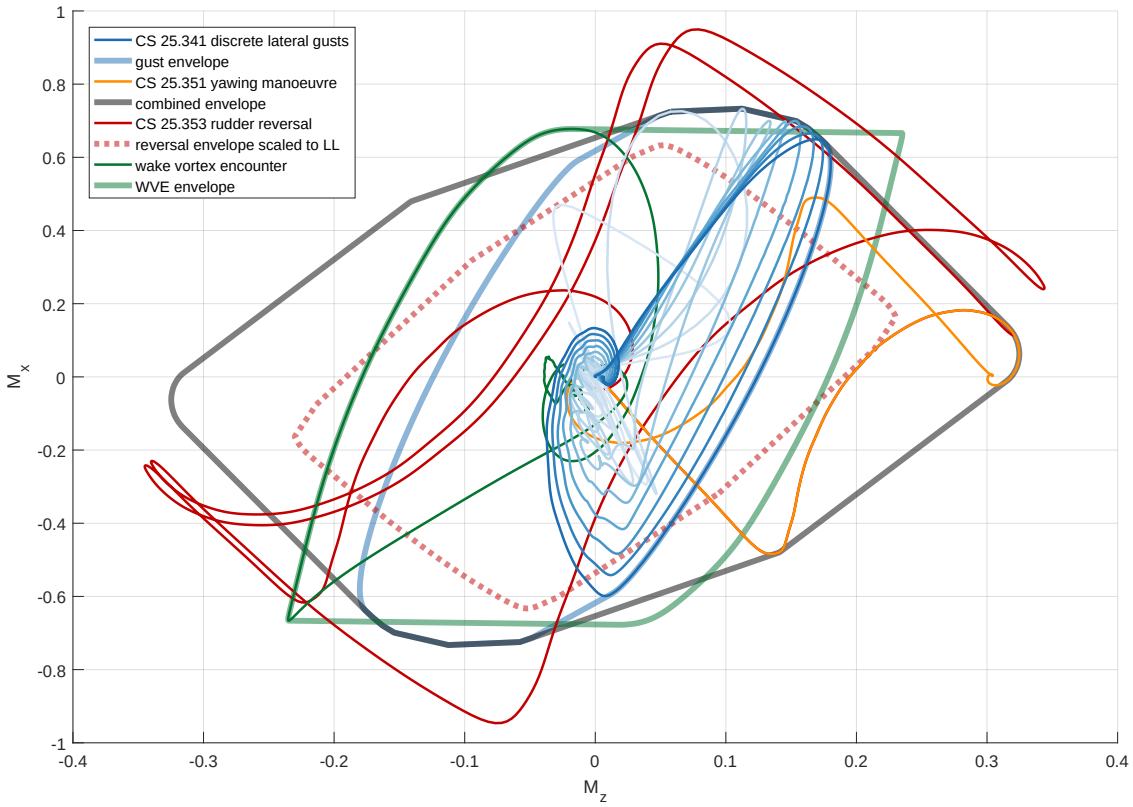

Figure 13: Correlated bending torsion moment loads for design loads and closed loop WVE

likely goes into saturation of the travel limitation unit. This excessive rudder action also causes a high torsional moment, which can be even larger than the loads induced by the yawing manoeuvre. When the rudder reversal load condition is considered, some increasing oscillations can be observed for the lower yaw damping gains. However, the fact that the resulting loads are considered ultimate, the reversal condition can be deemed uncritical. Hence, the vertical tail plane structure of lighter short range aircraft is more likely driven by gust loads. Figure 13 depicts the correlated bending and torsion moment envelopes at the VTP root for the discrete lateral gusts, yawing manoeuvre and the rudder reversal condition. The discrete lateral gusts are more prevalent compared to the heavier long range aircraft. With increasing yaw damping this trend fortifies.

The responses for rudder and right aileron deflections, respectively the sideslip and roll angle are shown in figure 14. The yawing manoeuvre condition shows a slight overshoot in sideslip angle. The reversal condition shows mild negative damping, resulting in the most severe sideslip angle, the resulting loads are considered ultimate.

When paying attention to the closed loop wake vortex encounter, the hefty control action becomes obvious. The rudder deflections even exceed those from the control reversal manoeuvre and are likely saturated by the rudder travel limiter. Also the aileron deflections go up to 35 deg. The resulting loads even exceed those of the rudder control reversal condition. The rolling motion however is considerably reduced to less than 15 deg (during the reported event, the roll angle went up to almost 60 deg).

Interesting to note is that when only the loads from control action by the autopilot is or alternatively only the loads induced by external disturbance are considered, the results are even more

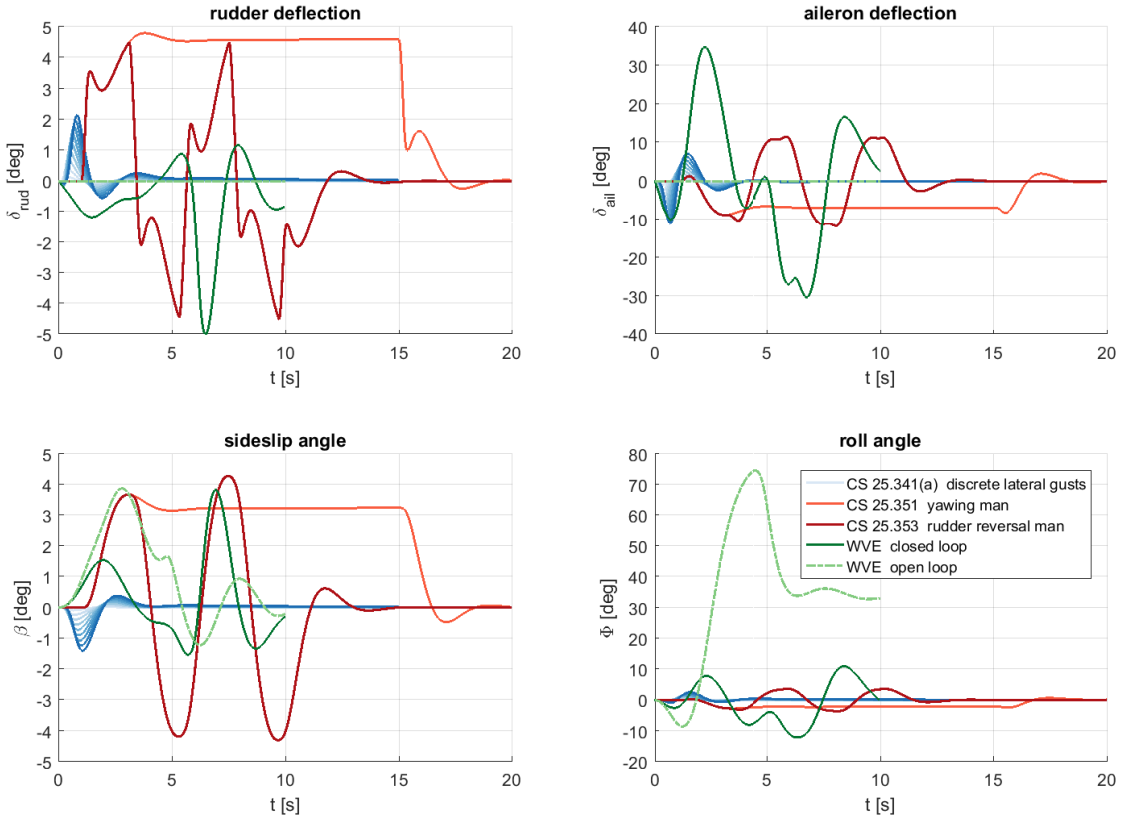

Figure 14: Responses for rudder/aileron deflections and sideslip/roll angle for design conditions and WVEs

severe. The wake vortex encounter is a true mixture of pilot manoeuvre and external gust field excitation and probably should be treated as such.

When examining the open loop wake vortex encounter, of course no control surface deflections are exerted. The roll angle shoots up to 75 deg during the event. A pilot would certainly not allow such an upset flight condition without counter measures. While the loads acting on the VTP are not large during the encounter, they might become excessive, when the aircraft has to be recovered from this upset flight state.

A more realistic scenario would be to used a pilot model with some level of pilot induced oscillation. Somewhere in between the near perfect compensation of the flight path disturbances of the flight controller and the simple open loop response with no control action at all. Of course the parameterization of the pilot model would grow the already immense parameter space for such wake encounter scenarios even larger.

6 SUMMARY AND CONCLUSION

An integrated model scheme to simulate manoeuvres and gusts of controlled flexible aircraft to determine design loads was presented. Complex scenarios with position and attitude dependent gust field such as wake vortex encounters are possible with this scheme. The unsteady aerodynamics can be accounted for by means of a physical rational function approximation. The present approach allows for a clear separation of quasisteady (important for manoeuvres) and unsteady aerodynamics (important for gusts and turbulence). The model equations are implemented for time domain simulations. This allows to easily account for nonlinearities in the aerodynamics or in the flight control laws, where rate and deflection limits are common.

A set of critical load conditions for the structural sizing of the vertical tail plane has been detailed: The yawing manoeuvre (CS 25.351) and the discrete lateral gust (CS 25.341(a)). Due to past flight incidents, where multiple reversing rudder pedal inputs made by pilots, a new load condition was introduced. The rudder control reversal condition (CS 25.353). The impact on the design loads of this new rule was assessed.

As all these load conditions are heavily influenced by the flight control laws, in particular by the yaw damper function and the rudder travel limitation unit. For a generic long range aircraft configuration the design torsion loads can be substantially reduced by overcritical damping of the yawing motion, since the maximum sideslip angle determines the maximum torsion moment on the VTP. Also the bending moment is reduced by the yaw damper during the yawing manoeuvre. The bending moment for lateral discrete gusts show a similar trend. For large yaw damping gains the bending moments from discrete gusts become critical, whereas for lower gains the bending moments due to manoeuvre are dimensioning.

The newly introduced rudder control reversal condition (CS 25.353) unsurprisingly results in higher loads, due to the fact that the rudder return command is full opposite instead of just return to neutral. Since the loads from the control reversal are considered ultimate, the sizing load levels are similar. In the particular case investigated, the VTP root bending moment is about 4% higher compared to the previous regulations without the new condition. This is for high gains of yaw damping.

Long range aircraft have a high mass moment of inertia about the vertical axis I_{zz}, i.e. yawing motion is not easily induced by gusts, however a sideslip overshoot behavior causes rather high loads. For the rudder control reversal condition with lower yaw damper gains this implies that reversing the rudder control three times at the maximum sideslip angle, a significant load builds up. The magnitude of the resulting loads is probably prohibitive for a lateral control law design with under-attenuated yaw damper gains.

Short range aircraft on the other hand have a rather low I_{zz}, i.e. gusts induce a rather high yaw rate, which for high gains causes large rudder deflections, even up to the limits of the RTLU. Compared to long range aircraft, short range models are more prone to loads from lateral discrete gust than yawing manoeuvres. The same statement holds for the new rudder control reversal condition, which seems to be well inside the conventional loads envelopes.

The introduction of the new rudder control reversal load condition was mainly motivated by wake vortex encounters, during which pilots made excessive or inappropriate use of the rudder. Therefore, simulations of a wake vortex encounters similar to a reported incident were set up. Then the closed loop aircraft encounter with wake at an angle of 3° was simulated. Rather large control surface deflections of the ailerons and rudder were commanded by the flight controller to keep course and attitude during the encounter. The resulting loads were of the same order of magnitude as the responses of the rudder control reversal condition. The conjecture of the new load condition is that the loads are predominantly caused by pilot action and not by the external disturbance itself. When examining the source of the loads during the wake encounter, it is shown that the loads due to pilot action and due to the vortex wind field are of the same order. The simulated encounter and the real incident are not completely comparable as there are no pilot induced oscillations in the simulation results. Further investigations of in-flight occurrences of wake vortex encounters and the loads induced are certainly worthwhile. A more realistic pilot model is required to reflect the overreaction when the pilot is startled by the sudden encounter.

The present integrated modelling approach allows to consider and assess various design load conditions already during the design of flight control laws. Typically flight control laws are designed with handling quality requirements in mind while structural loads only as an afterthought. The availability of models capable of accurately representing both, flight dynamics and loads analysis simultaneously could significantly improve the design process.

7 REFERENCES

[1] European Aviation Safety Agency (2018). *Certification Specifications for Large Aeroplanes CS-25*, vol. Amendment 22. EASA.

[2] Transportation Safety Board of Canada (2008). Encounter with Wake Turbulence, Air Canada Airbus A319-114 C-GBHZ. Tech. Rep. Aviation Investigation Report A08W0007, TSB.

[3] European Aviation Safety Agency (2017). Unintended or inappropriate rudder usage — rudder reversals. Notice of Proposed Amendment 2017-18 RMT.0397, EASA.

[4] Federal Aviation Administration (2018). Yaw Maneuver Conditions—Rudder Reversals. Notice of proposed rulemaking 18-04 FAA–2018–0653, FAA.

[5] Kier, T. and Looye, G. (2009). Unifying Manoeuvre and Gust Loads Analysis. In *International Forum on Aeroelasticity and Structural Dynamics*, IFASD-2009-106.

[6] Kier, T. (2011). An Integrated Loads Analysis Model including Unsteady Aerodynamic Effects for Position and Attitude dependent Gust Fields. In *International Forum on Aeroelasticity and Structural Dynamics*, IFASD-2011-052.

[7] Rodden, W., Taylor, P., and Jr., S. M. (1998). Further refinement of the subsonic doublet-lattice method. *Journal of Aircraft*, 9(10), 693–702. doi:10.2514/2.2382.

[8] Kier, T. (2013). An Integrated Loads Analysis Model for Wake Vortex Encounters. In *International Forum on Aeroelasticity and Structural Dynamics*, IFASD-2013-30C.

[9] Climent, H., Lindenau, O., Claverías, S., et al. (2013). Flight Test Validation of Wake Vortex Encounter Loads. In *International Forum on Aeroelasticity and Structural Dynamics*, IFASD-2013-27B.

[10] Claverías, S., Cerezo, J., Torralba, M. A., et al. (2013). Wake vortex encounter loads numerical simulation. In *International Forum on Aeroelasticity and Structural Dynamics*, IFASD-2013-30B.

[11] Hofstee, J., Kier, T., Cerulli, C., et al. (2003). A Variable, Fully Flexible Dynamic Response Tool for Special Investigations (VarLoads). In *International Forum on Aeroelasticity and Structural Dynamics*.

[12] Guyan, R. J. (1965). Reduction of stiffness and mass matrices. *Journal of Aircraft*, 3(2), 380. doi:10.2514/3.2874.

[13] Waszak, M. R. and Schmidt, D. K. (1986). On the flight dynamics of aeroelastic vehicles. In *AIAA Atmospheric Flight Mechanics Conference*, AIAA 86-2077. AIAA, pp. 120–133. doi:10.2514/6.1986-2077.

[14] M. R. Waszak and D. K. Schmidt (1988). Flight Dynamics of Aeroelastic Vehicles. *Journal of Aircraft*, 25(6), 563–571. doi:10.2514/3.45623.

[15] R. L. Bisplinghoff, H. Ashley, R. L. Halfman (1955). *Aeroelasticity*. Dover Publications Inc.

[16] Roger, K. L. (1977). Airplane math modeling methods for active control design. In *AGARD Structures and Materials Panel*, AGARD/CP-228. AGARD, pp. 4–1 – 4–11.

[17] Pistolesi, E. (1937). Betrachtungen über die gegenseitige Beeinflussung von Tragflügelsystemen. In *Gesammelte Vorträge der Hauptversammlung 1937 der Lilienthal Gesellschaft*.

[18] Harder, R. and Desmarais, R. (1972). Interpolation Using Surface Splines. *Journal of Aircraft*, 9(2), 189–191. doi:10.2514/3.44330.

[19] Edwards, J. W. (1979). Applications of Laplace transform methods to airfoil motion and stability calculations. In *20th Structures, Structural Dynamics and Materials Conference*, AIAA 1979-772. doi:10.2514/6.1979-772.

[20] Abel, I. (1979). An analytical technique for predicting the characteristics of a flexible wing equipped with an active flutter-suppression system and comparison with wind-tunnel data. Tech. Rep. NASA TP-1367, NASA LARC.

[21] Collar, A. (1946). The Expanding Domain of Aeroelasticity. *Journal of the Royal Aeronautical Society*, 50, 613–636.

[22] Lambregts, A. (1985). *Total energy based flight control system*. US Patent 4536843.

[23] Lambregts, A. A. (2013). TECS Generalized Airplane Control System Design–An Update. In *Advances in Aerospace Guidance, Navigation and Control*. Springer, pp. 503–534.

[24] Looye, G. (2013). TECS/THCS-based generic autopilot control laws for aircraft mission simulation. *Advances in Aerospace Guidance, Navigation and Control*.

[25] Pratt, K. and Walker, W. (1954). A revised gust-load formula and a re-evaluation of v-g data taken on civil transport airplanes from 1933 to 1950. Tech. Rep. NACA Report 1206, NACA.

[26] Joint Aviation Authorities (1989). *Joint Aviation Requirements JAR-25 Large Aeroplanes*, vol. Change 13. JAA.

[27] Joint Aviation Authorities (1994). *Joint Aviation Requirements JAR-25 Large Aeroplanes*, vol. Change 14. JAA.

[28] Barnes, T. J. (1990). Harmonization of us and european gust criteria for transport airplanes. In *17th International Congress of the Aeronautical Sciences, Stockholm, Sweden, September 9-14. 1990*. ICAS.

[29] European Aviation Safety Agency (2018). *Certification Specifications for Large Aeroplanes CS-25*, vol. Amendment 21. EASA.

COPYRIGHT STATEMENT